Aerospace Science and Technology 146 (2024) 108950

Contents lists available at ScienceDirect

Aerospace Science and Technology

journal homepage: www.elsevier.com/locate/aescte

Mid-fidelity numerical approach for the investigation of wing-propeller aerodynamic interaction

Claudio Niro, Alberto Savino, Alessandro Cocco, Alex Zanotti *

Politecnico di Milano, Dipartimento di Scienze e Tecnologie Aerospaziali, via La Masa 34, 20156, Milan, Italy

ARTICLE INFO

Communicated by Christian Circi

Keywords:
Aerodynamics
Mid-fidelity
Propeller-wing
Vortex particle method
eVTOL
Tiltrotor

ABSTRACT

The present activity was aimed to validate the capability of a vortex particle-based mid-fidelity aerodynamics code for the study of the aerodynamic interaction between a wingtip-mounted propeller and a wing with a 25% chord flap. The wing-propeller model considered in this work was widely investigated in literature, both by experiments and high-fidelity CFD simulations and represented a benchmark case for this kind of aerodynamic study, reproducing a typical feature of tiltrotors and electrical distributed propulsion aircraft configurations. In particular, in the present activity results of simulations performed with DUST, the mid-fidelity aerodynamic solver of Politecnico di Milano were compared in terms of wing loads distributions, propeller airloads and flow fields with both experimental data and high-fidelity CFD simulations available in literature. Analyses on the upstream and downstream effects on the propeller and wing performance showed that the benefits arising from the installation of a wingtip-mounted propeller can be correctly predicted. Moreover, the significant lift and propeller performance enhancement as well as the interactional flow physics characterizing this configuration were accurately captured by the solver. Generally, this validation activity showed a quite good agreement with high-fidelity CFD results, thus confirming that the mid-fidelity numerical approach implemented in DUST is suitable for the investigation of wing-propeller aerodynamics interaction. The quite lower computational effort required by this mid-fidelity approach, while maintaining accuracy with respect to high-fidelity CFD methods opens a new scenario for the preliminary stage of design of novel tiltrotor or eVTOL aircraft characterized by complex interactional aerodynamic mechanisms.

1. Introduction

In recent years, electrical vertical takeoff and landing (eVTOL) aircraft have emerged as a new and promising category of aerial vehicles. These aircraft utilize multiple rotors powered by electric battery technology, enabling vertical takeoff and landing and reducing dependence on traditional infrastructure such as runways. As a result, eVTOLs are expected to revolutionize urban and regional air mobility and become a major mode of transportation in the future [1–3]. The design of eVTOLs is driven by mission and safety requirements, resulting in the use of multi-rotor and multi-wing architectures. However, the aerodynamics of these configurations are dominated by intricate rotor-rotor, wing-rotor, and rotor-wing-airframe interactions that are difficult to simulate and predict. To address this challenge, mid-fidelity tools have emerged as an optimal trade-off between computational cost and desired accuracy, particularly to be used in the early stages of design. While classical high-fidelity computational fluid dynamics (CFD) methods can analyze these unsteady interactions, the resolution of wake dynamics requires high-order numerical schemes and mesh resolutions that are computationally expensive, making them unsuitable for design space exploration. Indeed, time-accurate RANS simulations of eVTOL aircraft are still computationally demanding and require significant resources. Therefore, high-fidelity CFD tools are often limited to a small number of detailed analyses and are unsuitable for the preliminary design of new eVTOL aircraft due to the large number of aerodynamic simulations required.

Academia and industry have therefore turned their attention to mid-fidelity codes to predict complex aerodynamic interactions. Numerous codes have been developed in recent years, offering a promising approach for eVTOL design and enabling the exploration of large design spaces while maintaining reasonable computational costs. For example, DLR's UPM [4] is an unsteady panel and free-wake code that was origi-

* Corresponding author.
E-mail addresses: claudio.niro@mail.polimi.it (C. Niro), alberto.savino@polimi.it (A. Savino), alessandro.cocco@polimi.it (A. Cocco), Alex.Zanotti@polimi.it (A. Zanotti).

https://doi.org/10.1016/j.ast.2024.108950
Received 23 May 2023; Received in revised form 30 January 2024; Accepted 30 January 2024
Available online 2 February 2024

Nomenclature

b	wing span	VPM	Vortex Particle Method
c	wing chord ..... m	V_∞	wind tunnel freestream velocity ..... m/s
c_b	blade chord ..... m	$x-y-z$	propeller-wing model reference system
CFD	Computational Fluid Dynamics	α	wing angle of attack ..... deg
C_l	sectional lift coefficient	ΔC_L	wing lift coefficient increase due to propeller installation ..... %
C_L	lift coefficient	ΔC_t	propeller thrust coefficient increase due to wing installation ..... %
C_p	pressure coefficient, $= P/(\rho n^3 D^5)$	δ_e	elevator deflection angle ..... deg
C_q	power coefficient $= Q/(\rho n^2 D^5)$	ε	downwash angle ..... deg
C_t	thrust coefficient $= T/(\rho n^2 D^4)$	ε_{C_L}	wing lift coefficient error with respect to CFD ..... %
D	propeller diameter ..... m	ε_{C_t}	propeller thrust coefficient error with respect to experiment ..... %
eVTOL	electrical Vertical Take Off and Landing aircraft	η	wing spanwise coordinate
J	advance ratio $= V_\infty/(nD)$	η_p	propulsive efficiency
n	angular velocity ..... rad/s	ψ	blade azimuthal angle ..... deg
Q	propeller torque ..... Nm	ρ	air density ..... kg/m^3
r	propeller blade radial coordinate	θ	blade pitch angle at 75% of the rotor radius ..... deg
R_p	propeller blade radius ..... m	ω_x	axial vorticity component 1/s
Re	Reynolds number	ω_x^*	normalized axial vorticity component $= \omega_x D/V_\infty$
t	blade thrust distribution, ... N/m		
T	propeller thrust ..... N		
u	axial velocity component ..... m/s		

nally designed for aeroacoustic simulations of helicopters but has since been applied to complex configurations like compound rotorcraft [5]. Moreover, the GENeral Unsteady Vortex Particle (GENUVP) is a software based on a panel method coupled with a VPM solver developed at the National Technical University of Athens (NTUA) for both aerodynamic and aeroacoustic simulations of rotorcraft [6]. In particular, vortex particle method (VPM) [7] is widely used in mid-fidelity codes to enhance the evaluation of aerodynamic characteristics of rotors and rotor-airframe interactions. Recent studies showed the effectiveness of VPM for rotorcraft applications, such as the work by Su et al. aimed at the analysis of the aerodynamic characteristics of an electrically controlled rotor using a viscous VPM-based model [8]. An unsteady aerodynamic analysis method based on VPM was recently developed for the investigation of the complex wake of coaxial rotors in the work by Tan et al. [9], while a vortex-based approach coupled with a viscous boundary model was used by the same authors to investigate complex rotorcraft-to-rotorcraft interference problems [10]. Moreover, Alvarez et al. [11] recently published a survey on the use of their VPM-based interactional aerodynamics solver FLOWUnsteady for both multirotor aircraft and wind energy applications.

Nevertheless, further validation studies need to be conducted in order to verify to which extent and in which flight conditions the mid-fidelity can be used and gives good useful results, particularly to face the challenge introduced by the novel complex architectures of Advanced Air Mobility (AAM) configurations characterized by interactions of propulsion systems with wing-airframe. Overall, the interaction between the propulsive system and airframe is a critical consideration in aircraft design and proper integration can result in significant performance gains. As aircraft designs continue to evolve, ongoing research in this area will undoubtedly lead to further improvements in the integration of propulsion systems with airframes.

In this scenario, the present work is aimed to the validation of the mid-fidelity solver DUST of Politecnico di Milano [12] for the investigation of the wing-propeller aerodynamic interaction in a tip-mounted configuration. Great interest grows indeed in the recent years towards the aerodynamic interaction between wing-tip mounted propellers and lifting surfaces, thanks to the growing popularity of eVTOL technology. One of the earliest experimental studies on this topic was conducted by Sinnige et al. [13,14] aimed to address the lack of comprehensive analyses of the aerodynamic interaction effects by providing a detailed aerodynamic analysis of the wingtip-mounted configuration. The study involved integral and local force measurements and comprehensive flow field evaluations through an experimental approach. Recently, Stokkermans et al. [15] explored the use of RANS solvers for simulating wingtip-mounted propellers with the goal of reducing computational costs while accurately capturing propeller-wing interactions. To address this issue, the authors evaluated the accuracy of RANS simulations for this particular configuration and explored the use of actuator-disk (AD) and actuator-line (AL) models. Last year, Van Arnhem in his doctoral dissertation [16] exploited the effects of a wing tip mounted propeller mounted on a tailplane but also on the complete aircraft.

In the present activity the wing-propeller configuration tested in the experimental campaign by Sinnige et al. [13] is considered for numerical simulations performed with DUST. The goal of the present work is to validate the capabilities of mid-fidelity tools for the preliminary design of novel aircraft architectures characterized by complex wing-propeller aerodynamic interactions, as done in recent literature by Stokkermans et al. [15] for classical high-fidelity CFD methods on the same test case. With this aim, DUST simulation results will be comprehensively discussed and compared with both experimental and CFD data available in these recent literature works to fully highlight the limits and benefits of this mid-fidelity approach for the study of such complex interactional aerodynamics test cases.

The paper is organized as follows. Section §2 provides the description of the numerical model built in DUST for the simulations of the wing-propeller configuration. Section §3 presents the comparison and discussion of the DUST simulations results with experimental and high-fidelity CFD data available in the literature for the same test case. Conclusions are drawn in Sec. §4.

2. Numerical model

2.1. Description of the mid-fidelity aerodynamic solver DUST

DUST is an open-source software developed by Politecnico di Milano to simulate the interactional aerodynamics of unconventional rotorcraft configurations. The code is released as free software under the open-source MIT license. The code relies on an integral boundary element formulation of the aerodynamic problem and on a vortex particle model [7,17] of the wakes. This choice naturally fits the Helmholtz decomposition of the velocity field from a mathematical point of view and avoids

the numerical instabilities occurring with connected models of the wake in practice. A numerical model in DUST can be built using several components connected to user-defined reference frames, whose position and motion can be defined hierarchically. Different aerodynamic elements allow for different model fidelity levels, ranging from lifting line elements to zero-thickness lifting surfaces and surface panels for thick solid bodies. In particular, lifting line elements naturally represent viscous effects since they rely on tabulated aerodynamic lift, drag, and moment coefficients of two-dimensional sections as functions of the relative velocity direction and magnitude, calculated as the projection of the computed three-dimensional velocity on the airfoil sections. In particular, the circulation of the lifting line is determined as the solution of a non-linear problem, connecting the circulation with the tabulated aerodynamic coefficients of its lifting two-dimensional sections, following a Γ-method solver [18]. In Γ-method, circulation is computed using tabulated sectional lift and its analytical expression from Kutta-Joukowski theorem.

The simulation is evolved in time with a time-stepping algorithm, solving in sequence the Morino-like problem [19] for the potential part of the velocity field, the nonlinear problem for the lifting lines, and updating the rotational component of the velocity field integrating the Lagrangian dynamical equations of the wake particles. A detailed mathematical description of the formulation implemented in DUST is reported in [20]. DUST was also coupled with the multibody solver MBDyn to obtain a fast aeroelastic solution for rotorcraft configurations and has the capability to model the deflection of control surfaces as described in [21]. This latter capability was thoroughly used in the present work to reproduce the deflection of the flap for the considered wing-propeller configuration.

2.2. Description of the wing-propeller model

The propeller geometry used in this study is the same used on the de Havilland DHC-2 Beaver. The propeller called “TUD-PROWIM” was specifically designed and manufactured by TU Delft for investigating propeller-wing interaction effects in low-speed wind tunnel tests [13] and was extensively used for numerical aerodynamic tools validation [15,22,11]. The propeller features four blades and has a rotor radius $R_p = 0.1185\ m$ with a pitch angle $\theta = 23.9°$ at 75% radius. A 3D scanning of the blade enabled to obtain a CAD drawing (available from [13]) that was used to build the numerical model of the propeller. In particular, blade airfoils were extracted from the CAD on 17 spanwise sections, thus angle of attack distributions were reconstructed to reproduce the correct blade geometry. As the present blades are unswept, no corrections on effects related to robust three-dimensionality of the flow are considered. Nevertheless, for high sweep angles, lifting line method exhibits some limitations and require corrections, particularly at high lift coefficients, i.e. near to stall, as investigated and shown in Gori et al. [23]. Radial distributions of the propeller blade chord and pitch angle were presented in Fig. 1.

Considering the blade sections extracted from the CAD, ten different NACA airfoil profiles were selected to properly model the propeller blade geometry. The blade airfoil distribution is reported in Table 1. Propeller blades were modeled using lifting line elements [12]. The sectional tabulated aerodynamic coefficients were calculated by XFOIL simulations [24], while the Viterna method [25] was used to calculate the behavior of the sectional aerodynamic loads coefficients in the range between ±180° angle of attack. A spatial convergence study leads to the selection of a number of 34 equally spaced lifting line elements in the radial direction to model each of the propeller blades. DUST simulations were performed considering a length of 8 propeller revolutions with a time discretization of 5° of blade azimuthal angle. Details about time and spatial convergence studies were not here reported for the sake of consistency, but are available in Niro’s M.Sc. degree dissertation [26].

The complete test case includes a straight, untapered wing with 0.240 m chord length, 0.292 m span, and a constant symmetric NACA

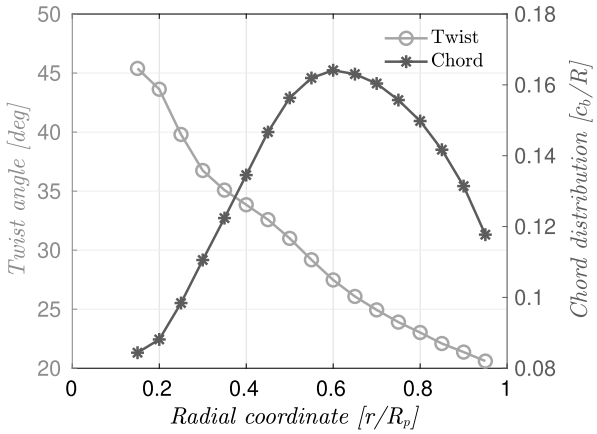

Fig. 1. Radial distributions of the propeller blade chord and pitch angle.

Table 1
TUD-PROWIM blade airfoil radial distribution used to build DUST propeller model.

	from [%R]	to [%R]
NACA 0460	15	25
NACA 2246	30	30
NACA 4428	35	35
NACA 4424	40	40
NACA 4416	45	45
NACA 4413	50	50
NACA 4411	55	55
NACA 2411	60	60
NACA 2410	65	65
NACA 2409	70	70
NACA 2408	75	100

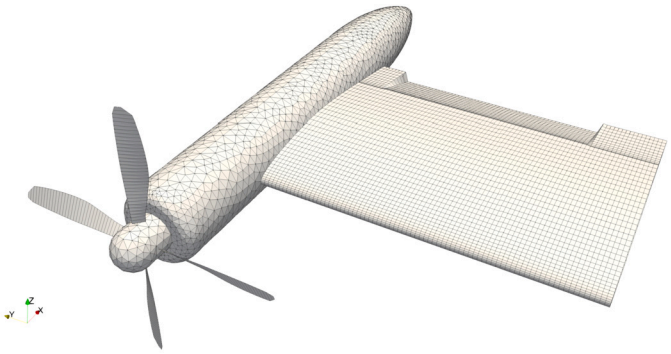

Fig. 2. The DUST mesh for the complete wing-propeller model.

64_2A015 airfoil. The wing is equipped with an integrated 25%-chord plain flap, here acting as an elevator. The wing was modeled with surface panels. A spatial convergence study leads to the use of a discretization of 85 panels in a spanwise direction and 45 panels in a chordwise direction. Analogously to the propeller model, the results of the wing spatial convergence study are reported in Niro’s M.Sc. degree dissertation [26]. The test case object of this study is completed by a nacelle that was modeled by an unstructured mesh composed of 4126 surface panel elements. The wing-nacelle geometry was available from a CAD drawing reported in [13]. The mesh of the complete numerical model built for DUST simulations along with the reference system is shown in Fig. 2.

The wind tunnel model to be reproduced in this work involved a wing-tip propeller mounted on a wing directly attached to the test section floor. Thus, the wall effect was simulated in the numerical model by extending the wing by half of the wind tunnel model span, also in-

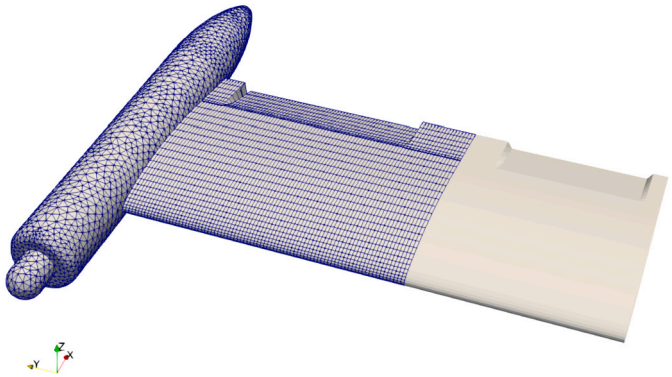

Fig. 3. Overview of the DUST numerical model including the extended portion of the wing used to model the wall effect.

cluding the flap with the same chordwise characteristics (see Fig. 3). This solution enabled to avoid that the circulation would not decay to zero in correspondence with the wall section and was verified by a preliminary numerical study performed with DUST on the single wing configuration. Indeed, this study showed that the extended wing model with deflected flap is suitable to obtain a quite good agreement between DUST results and CFD data [22] for the local spanwise wing loading in the region corresponding to the wind tunnel floor. Results of this study are not reported for the sake of consistency but can be found in Niro's M.Sc. degree dissertation [26]. An image propeller positioned on the extended wing region was not considered to limit the computational effort required by the numerical model. Indeed, the whole numerical activity was performed using a commercial personal laptop. The complete model simulation required about 10 hours of computational time using a laptop equipped with a Intel® Xeon E3-1505M with 4 physical core.

3. Results and discussion

The outcome presented in this section are based on the extensive research conducted by TU Delft, as documented in [13,15,22,27]. In these works, a comprehensive analysis of the present test case using high-fidelity CFD simulations and experimental wind tunnel testing is given, thus providing a robust foundation for the validation of the DUST methodology. In particular, a comparison of DUST simulation results with experimental and high-fidelity CFD data is presented in the following starting from the single propeller configuration to the complete model with the propeller installed on the wing.

3.1. Single propeller results

Fig. 4 illustrates a comparison between thrust and torque coefficients at different advance ratios obtained by DUST simulations and CFD data computed by Sinnige et al. [14]. Results show a high level of agreement along almost the entire range of advance ratio J tested, with the only exception at small advance ratios where DUST curves show a plateau. A quantitative comparison of thrust coefficient is presented in Table 2 for advance ratio $J = 0.8$, showing that a similar percentage error, in the order of 3%, with respect to the experimental data can be found for both DUST and high-fidelity CFD approach.

Further validation of the DUST model was provided by the comparison of the propulsive efficiency with both experimental and CFD data. As can be observed in Fig. 5 DUST model accuracy is even more pronounced when compared to experimental data and provides the same accuracy as CFD simulations. This outcome provides further evidence of the reliability of the mid-fidelity solver for the evaluation of propellers' aerodynamic performance.

In addition to performance coefficient comparison, a more in-depth analysis of the DUST propeller model was conducted by examining the

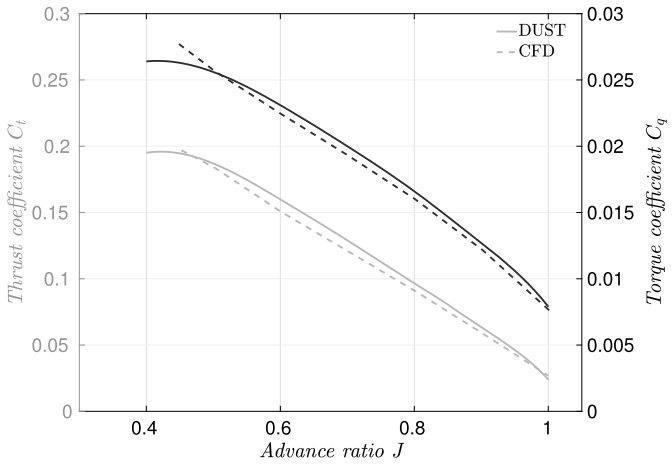

Fig. 4. Thrust and torque coefficients for single propeller configuration computed with DUST and compared with URANS simulations by [14] at different advance ratios J.

Table 2
Thrust coefficient C_T for single propeller configuration at $J = 0.8$. Error ε_{C_t} is computed as percentage w.r.t. experimental data computed by Sinnige et al. in [13].

Configuration	Model	C_t [-]	Error ε_{C_t} [%]
Single Propeller	DUST	0.096	2.1
	CFD	0.091	3.2
	Experimental	0.094	-

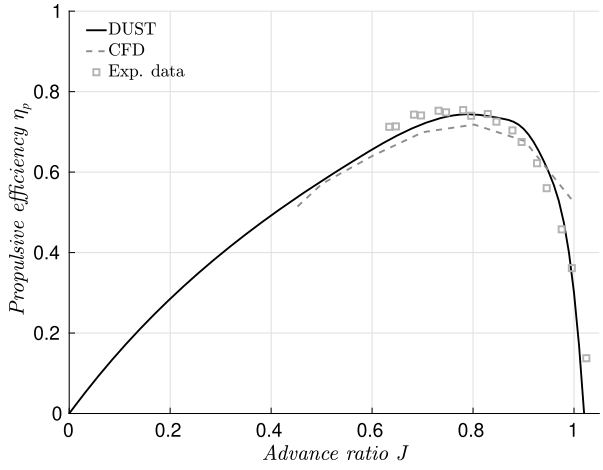

Fig. 5. Comparison of Propulsive efficiency η with URANS simulations [14] and experimental data [13] at different Advance ratios J.

blade thrust radial distribution. In particular, Fig. 6 shows the comparison between the sectional thrust distribution curves evaluated along radial coordinate of the blade normalized with propeller total thrust computed respectively by DUST and CFD. The curve comparison indicates again a quite good agreement between DUST and CFD with the only exception at blade root, in particular for $r/R_p \leq 0.4$, where possible local flow separation due to the bluffed body geometry and the high pitch angle characterizing this region could occur. This leads to a higher uncertainty in the calculation of the unsteady loading, as shown also by the higher spread of the CFD solution in this region presented by Stokkermans et al. [15].

Considering now flow field comparison, a snapshot of the instantaneous flow field obtained from DUST simulation is compared with high-fidelity CFD results from URANS simulations by Stokkermans et al. [15] in Fig. 7. The tip vortices introduce the largest gradients in the

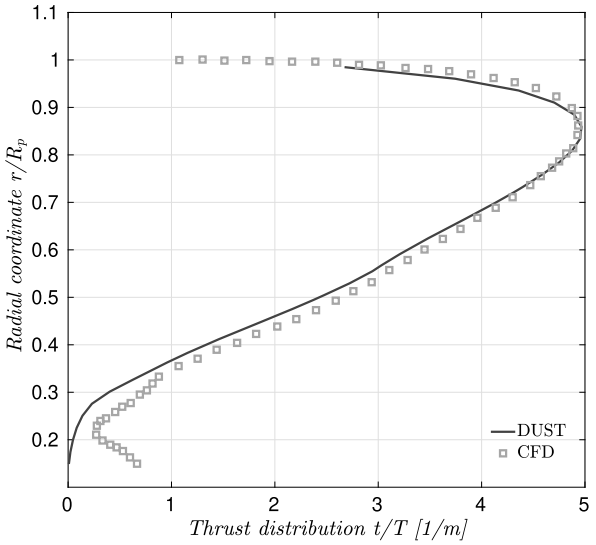

Fig. 6. Propeller blade thrust radial distribution at $J = 0.8$ normalized with respect to total propeller thrust, CFD data from [15].

flowfield, leading to fluctuations of more than 50% of the freestream velocity. The comparison of DUST flow field results with those obtained from CFD indicates a high degree of similarity. Specifically, the vortices intensity computed by DUST is quite similar to CFD. Nevertheless, the boundary layer region the wall is not adequately modeled in DUST, resulting in a less significant reduction of axial velocity than in the CFD case. Nonetheless, DUST is capable of capturing the overall flow physics characterizing the region past the propeller disk.

A more quantitative comparison of the flow field is provided by axial velocity profiles centered with respect to the second, fourth and sixth tip vortices shown in Fig. 7, i.e. along white lines indicated by A, B and C. DUST results show a good agreement with CFD data. In particular, DUST represents correctly the flow physics past the propeller disk by capturing the induced flow in the upstream direction at the location of the tip vortices with a similar degree of accuracy with respect to CFD. Indeed, both the high- and mid-fidelity numerical approaches underestimate the intensity of tip vortices, as shown by the lower peak-to-peak velocity gradients near $r/R_P \approx 1$ with respect to experimental data provided by Sinnige et al. [13] (see Fig. 8). Going into details, DUST provides a better representation of the tip vortices positioning with respect to CFD. Indeed, the peak of the axial velocity calculated by CFD simulations is shifted slightly downward with respect to experiments, while a quite good alignment is observed on both section A and B with DUST representation. A similar behavior is also observed on section C, but in this case the experimental data are not available for comparison. On the other hand, as previously anticipated by the flow fields comparison, the higher discrepancies between DUST and both CFD and experimental velocity profiles are found close to the nacelle, due to intrinsic modeling limitation of the boundary layer region. Indeed, as can be seen on section A, DUST underpredicts the axial velocity at the inboard region of the velocity profiles, particularly for $r/R_P \leq 0.4$.

3.2. Wing-propeller configuration

The operating conditions simulated by DUST for the complete wing-propeller model are reported in Table 3.

3.2.1. Effect of wing installation on propeller airloads

Results discussion started considering the mutual interactional effects provided by the installation of the wing and propeller, respectively on the propeller and wing aerodynamic loads.

Table 4 shows the comparison of the averaged propeller thrust coefficient C_t for the single and installed configurations. An increase in the

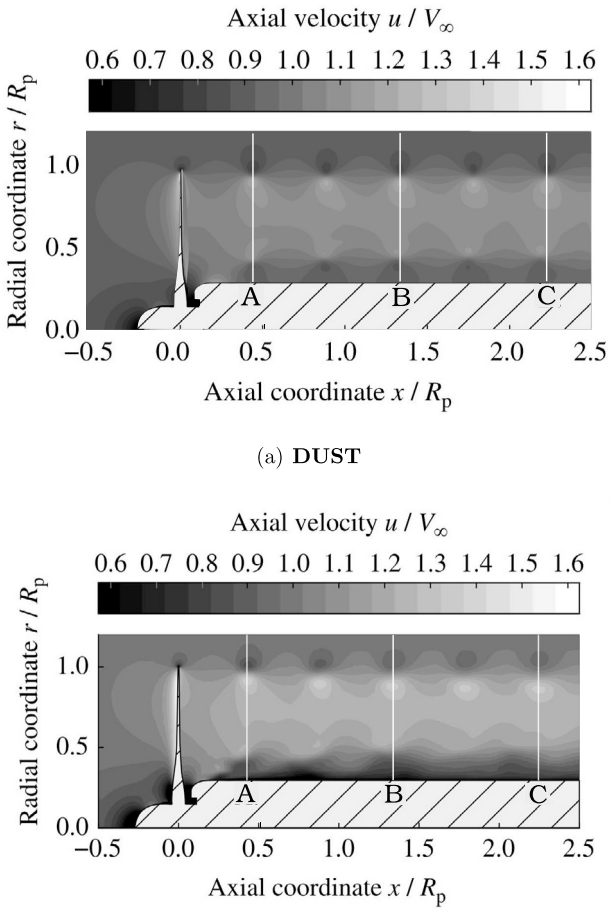

(a) **DUST**

(b) **CFD** [15]

Fig. 7. Axial-radial contour plots of phase-locked axial velocity.

Table 3
Selected operating conditions for the wing-propeller DUST simulation.

α [°]	V_∞ [m/s]	J [-]	Angular velocity n [rad/s]	δ_e [°]	Re [-]
0	40	0.8	1325	10	6.5×10^5

Table 4
Effects on the propeller thrust coefficient C_T due to the wing installation at $\alpha = 0°$ and $\delta_e = 10°$. Error ε_{C_t} is computed w.r.t. experimental data by Sinnige et al. in [13].

Configuration	Model	C_t [-]	ε_{C_t} [%]	ΔC_t [%]
Single propeller	DUST	0.096	2.9	-
	CFD	0.091	3.0	-
	Experimental	0.094	-	-
Installed propeller	DUST	0.105	8.6	+9.4
	CFD	0.098	2.1	+7.6
	Experimental	0.096	-	+2.2

propeller thrust due to wing installation is apparent. The experimental C_t value for the installed propeller configuration is better captured by CFD, but both DUST and CFD overestimate the ΔC_t increase due to wing installation with respect to experiments. The difference of the numerical ΔC_t with respect to experimental results can be due to the use of a transition strip in the experiments conducted by Sinnige et al. [13], which induced a forced laminar-to-turbulent boundary layer transition. Nevertheless, DUST effectively captures the performance enhancements resulting from propeller integration with the wing and nacelle, particularly calculating an increase in propeller performance quite similar to

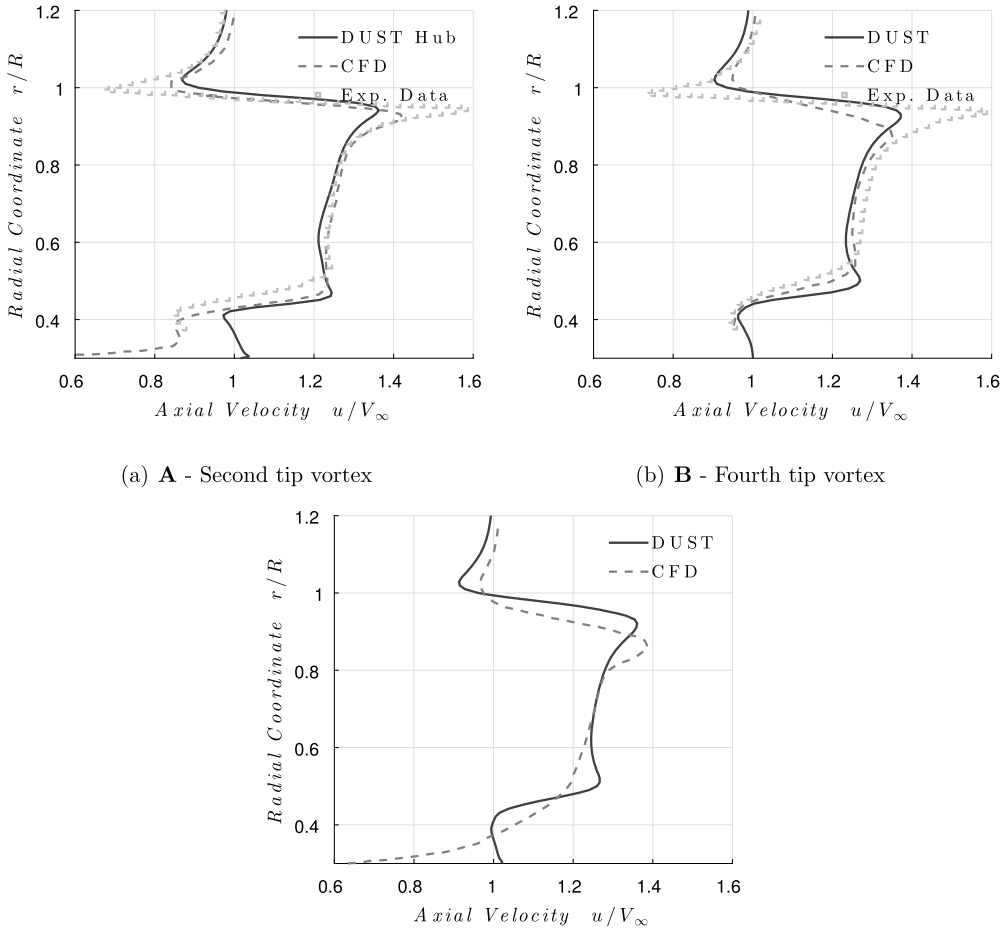

(a) **A** - Second tip vortex

(b) **B** - Fourth tip vortex

(c) **C** - Sixth tip vortex

Fig. 8. Comparison of axial velocity profiles past the propeller. URANS CFD from Stokkermans et al. [15].

CFD computation. This result is quite interesting considering the use of a mid-fidelity approach for the preliminary design stages, which necessitates a fast and accurate evaluation of the effects of possible airframe integration on propeller aerodynamic performance.

The propeller blade sectional azimuthal thrust distribution computed for elevator deflections $\delta_e = 10°$ shown in Fig. 9 can be helpful to explain the performance enhancement observed for the installed propeller configuration. First of all, the contour comparison showed an excellent agreement of the sectional loads between DUST and high-fidelity URANS simulations, thus confirming the mid-fidelity code accuracy for the evaluation of the installed propeller performance. The sectional loads' contours reveal that a positive elevator deflection leads to an increase in thrust contribution in the region where the propeller blades are near the wing's leading edge, i.e., $\psi = 0°$. In this region, the wing blockage and the net upwash caused by the wing-bound vortex and the trailing vortex system result in an upstream effect.

The upwash is in the same direction as the propeller's rotation direction, thereby reducing the local angle of attack of the blade sections. The propeller thrust increase is primarily due to the locally reduced axial velocity caused by the wing blockage effect, which results in a decreased effective advance ratio for the blade sections. Moreover, at $\psi = 90°$ and $\psi = 270°$, the blade loading is mainly influenced by the wing-bound vortex shed by the nacelle. On the pressure side of the wing ($\psi = 90°$), there is a local reduction of inflow velocity to the propeller, while on the wing suction side, there is an increase in inflow ($\psi = 270°$), leading to an increase in propeller loading in this region.

Table 5
Effects on the system lift coefficient C_L arising from the integration of the propeller into the airframe at $\alpha = 0°$ and $\delta_e = 10°$. Error ε_{C_L} is computed w.r.t. CFD data computed by Stokkermans et al. [15].

Configuration	Model	C_L [-]	ε_{C_L} [%]	ΔC_L [%]
Single wing	DUST	0.198	1.0	-
	CFD	0.200	-	-
	Experimental	0.189	5.5	-
Wing with installed propeller	DUST	0.244	5.4	+23.3
	CFD	0.259	-	+29.5
	Experimental	0.257	0.8	+36.0

3.2.2. *Effect of propeller installation on wing airloads*

Table 5 presents the quantitative effect of the installed propeller on the wing lift coefficient C_L evaluated from experiments and simulations. For the single-wing test case, DUST shows a quite good agreement with CFD, showing less than 1% error with respect to high-fidelity methods. The significant differences obtained from computations with respect to experimental results are due to the use of transition strip in the experiments conducted by Sinnige et al. [13], thus in Table 5 the error values ε_{C_L} are evaluated with respect to CFD by Stokkermans et al. [15] considered as reference. When the propeller is installed, a noticeable lift enhancement of the wing can be observed from both experimental and numerical results. In particular, a small underestimation is observed for DUST results with respect to both CFD and experimental data. This occurs due to the fact that DUST fails to accurately capture

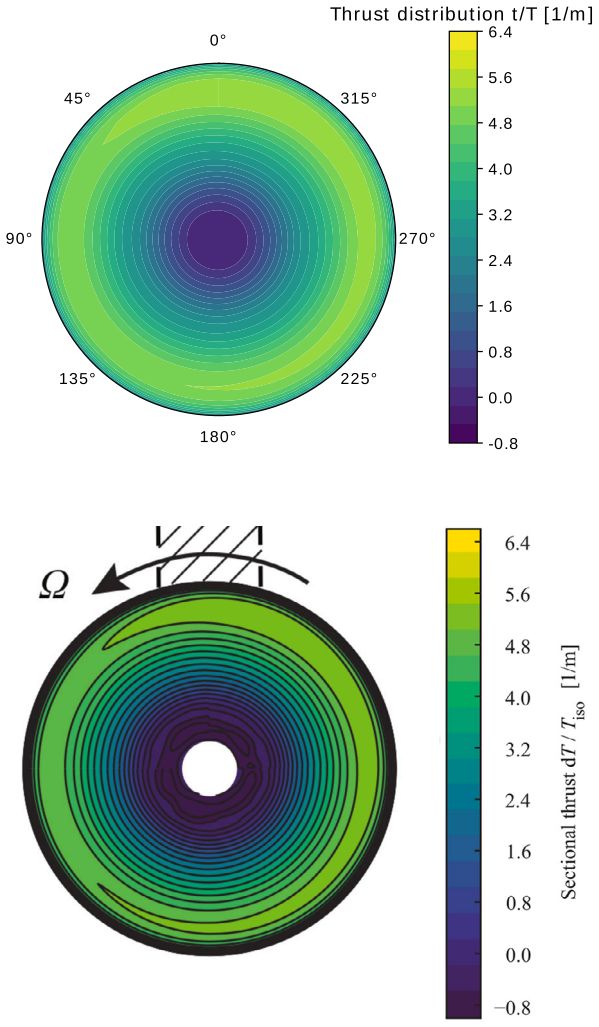

Fig. 9. Propeller blade sectional azimuthal thrust distribution computed with DUST (top) and with URANS CFD by Van Arnhem [16] (bottom).

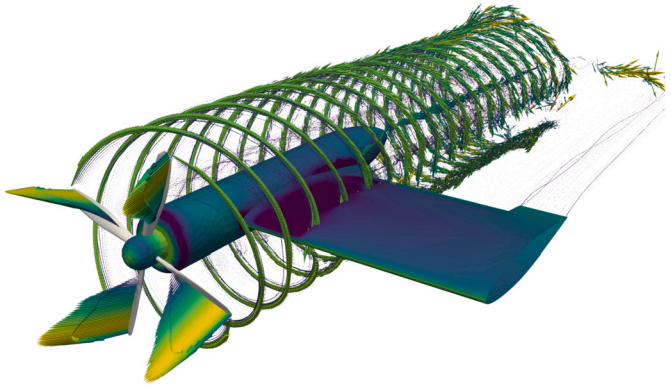

Fig. 10. DUST solution visualization of the complete wing-propeller model at $\delta_e = 10°, \alpha = 0°$ and $J = 0.8$.

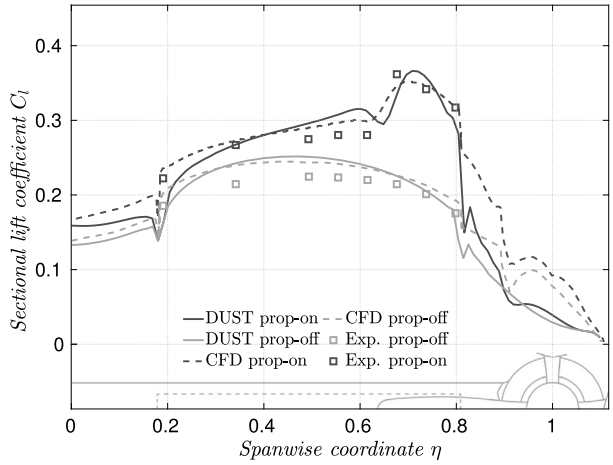

Fig. 11. Sectional lift coefficient distribution at $\alpha = 0°$ and $\delta_e = 10°$ for the complete model with and without the installation of the propeller.

the nacelle contribution to the system lift coefficient, as will be discussed later. Despite these limitations, DUST shows the capability to correctly capture the beneficial effect of installing a propeller in wingtip configuration on the airframe, providing a ΔC_L increase similar to high-fidelity CFD computation.

The analysis of the span-wise loading and pressure distribution on the wing enables us to achieve a more detailed insight into the wing lift enhancement mechanism due to propeller installation. In particular, Fig. 10 shows a visualization of the DUST solution for the complete wing-propeller model. Pressure distribution over the wing indicates that the propeller slipstream investing the wing induces a modification of the inboard wing loading, resulting in upwash and a local lift increase compared to the propeller-off case, as will be discussed later.

Fig. 11 shows the comparison of the spanwise sectional lift coefficient distribution with and without the installation of the propeller. The sectional lift coefficient curves show a lift increase with respect to the propeller-off condition that can be attributed to the inboard-up rotation of the propeller providing an upwash and a dynamic pressure increase on the wing spanwise part washed by the slipstream ($0.6 \leq \eta \leq 0.8$). Results obtained by DUST capture this effect and are in good agreement with those obtained by CFD along almost all the wing span, as well as are consistent with those obtained from experiments. The maximum sectional lift value calculated by DUST with a propeller on is quite similar to the experimental one and slightly shifted outboards, while DUST prediction for the lift coefficient over the flap deflection zone has a steeper increase compared to CFD and experimental data. Sectional lift obtained in the nacelle region is quite underestimated with respect to CFD, thus justifying the lower values of the integral wing lift increase computed by DUST with respect to high-fidelity computation (see Table 5).

The beneficial effect on wing performance arising when the propeller is installed into the airframe is further demonstrated by the pressure distributions comparison shown in Fig. 12 at two different spanwise locations, one at the edge of the propeller slipstream and a second into the propeller slipstream. A more pronounced suction peak near the leading edge appears with a propeller on as a result of the combination of the dynamic pressure rise and upwash due to the slipstream, as can be seen in Fig. 12. The pressure coefficient at the stagnation point is greater than unity due to the wing section's location into the propeller slipstream, as freestream dynamic pressure was used to calculate the pressure coefficient as done by [15]. DUST outcomes are in quite good agreement with measurements and CFD results confirming the suitability of the mid-fidelity numerical model. Large pressure fluctuations occur at the trailing edge region due to the flap deflection, well captured again by DUST simulation.

3.2.3. Flow fields analysis

Fig. 13 displays the distribution of the normalized axial vorticity ω_x^* within the slipstream region on a transversal slice parallel to the wing disk at $1.5c$ downstream the trailing edge of the wing compared to experimental measurements obtained using Particle Image Velocimetry (PIV) reported by van Arnhem [16].

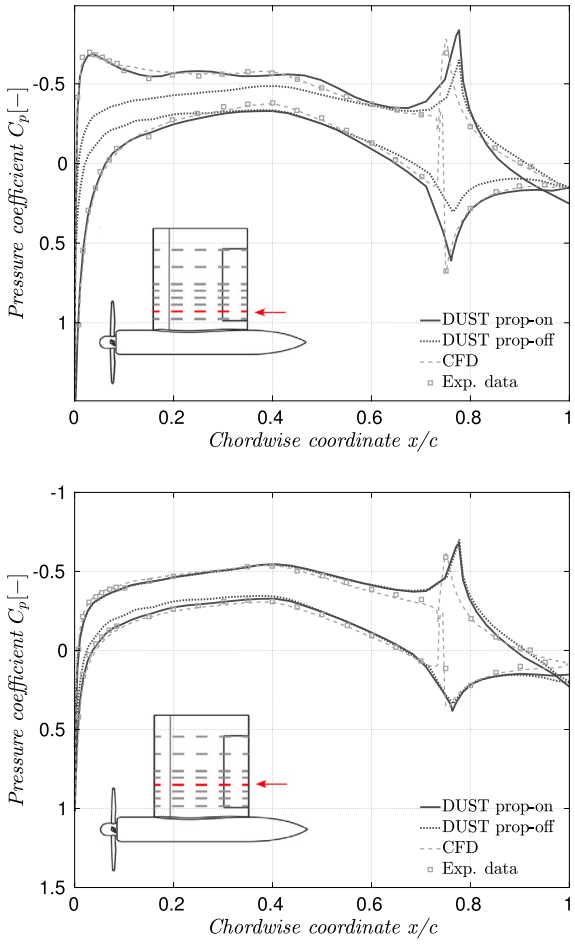

Fig. 12. Pressure distribution on wing sections at $\alpha = 0°$ and $\delta_e = 10°$ with and without the installation of the propeller. CFD and experimental data for propeller-on condition.

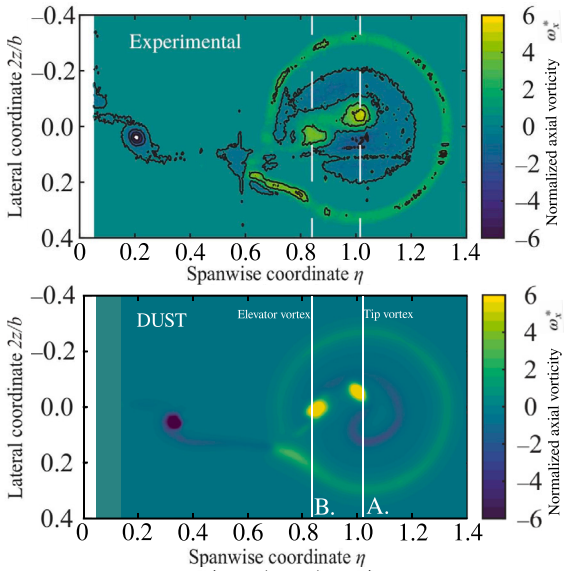

Fig. 13. Comparison of the normalized axial vorticity component ω_x^* on a slice at $1.5c$ downstream the trailing edge of the wing, PIV results from [16].

The inboard and outboard elevator edges are observed to shed vortices at $y/b \approx 0.2$ and $y/b \approx 0.8$, while a blade tip vortex is observed at $y/b \approx 1$. The rotor slipstream is shown to envelop this tip vortex

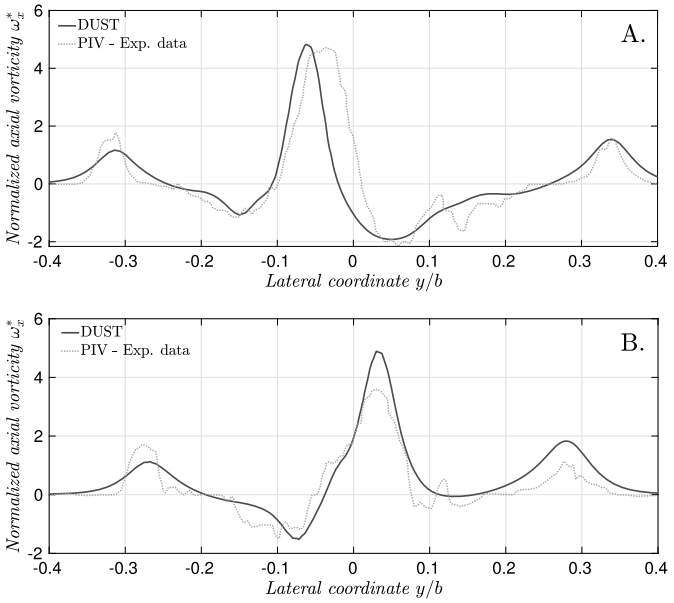

Fig. 14. Comparison of the normalized axial vorticity component ω_x^* along tip vortices sections, PIV results from [16].

and is distorted by the wing surface. This behavior exposed by PIV is well captured by DUST simulation. A further quantitative comparison is provided by vorticity profiles along the elevator vortex and tip vortex (sections A. and B. indicated in Fig. 13) and shown in Fig. 14. The quite good agreement of the vorticity profiles with experimental measurements indicates DUST capability to properly capture the flow physics of the interactions between the propeller wake and the wing surface.

Moreover, Fig. 15 presents the comparison of the downwash angle field behind the propeller, showing again a quite good agreement of DUST results with CFD and experiments in terms of flow field representation.

A quantitative comparison is also provided in Fig. 16, showing the downwash angle distributions on the slices A and B depicted in Fig. 15. The general behavior of the CFD and experimental distribution of the downwash is well captured by DUST, even with some exceptions of the peak-to-peak amplitudes of slice A, while a quite good agreement is found on slice B.

4. Conclusions

The present work described a numerical investigation aimed at the validation of the capabilities of a mid-fidelity VPM-based aerodynamic solver to analyze the complex aerodynamic interaction that occurs when a tractor tip-mounted propeller is installed on a wing with a deflected flap. The selected test case was the object of a comprehensive experimental campaign and was also considered in recent literature for the validation of RANS methods. The present work provides novel insights to industrial and scientific communities about the use of numerical methods requiring a lower computational effort for the simulation of complex propeller-based aircraft configurations.

In particular, the first result of this work was that the DUST mid-fidelity solver can provide the same level of accuracy with respect to high-fidelity CFD in terms of calculation of the aerodynamics performance curves of a single propeller as well as for the evaluation of the main flow physics characterizing the propeller operation. Then, the study focused on propeller integration onto the airframe. DUST simulations show the code's capabilities to capture the main interactional flow features arising between the unsteady flow induced by the propeller and the presence of the wing with deflected flap. Indeed, the DUST solver was capable to calculate the variation of propeller aerodynamic performance due to wing installation with similar accuracy provided by

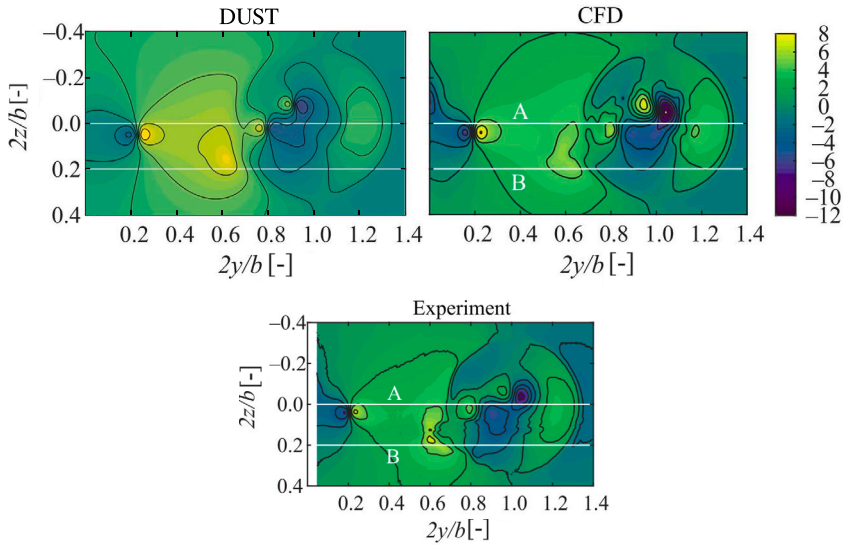

Fig. 15. Comparison of the downwash ε on a vertical slice at $1.5c$ behind the trailing edge of the wing, PIV and CFD results from [16].

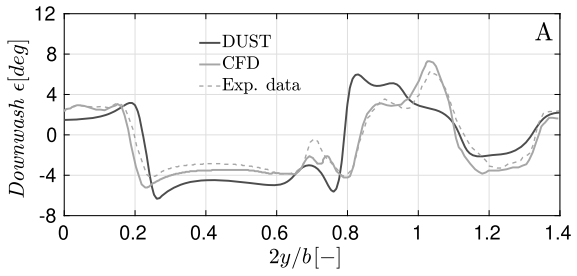

(a) Downwash ε in the A-plane

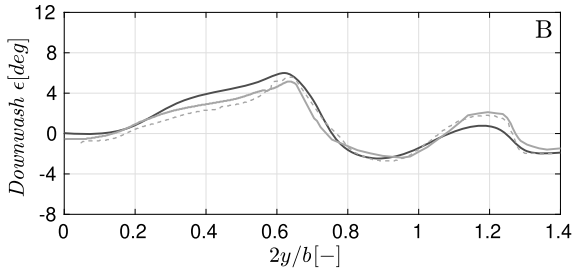

(b) Downwash ε in the B-plane

Fig. 16. Slices of downwash angle distributions on the two different sections A. and B. depicted in Fig. 15, PIV and CFD results from [16].

high-fidelity CFD, as well as to compute the effects of propeller blowing on wing load distribution. Higher discrepancies between mid-fidelity calculations and CFD were locally observed considering wing loading in the nacelle region due to some limitations of the mid-fidelity approach to solve bluff bodies aerodynamics with high accuracy. On the other hand, flow physics related to the interaction of the propeller slipstream tip vortices with the wing surface equipped with deflected flap is very well reproduced by the DUST model, as good agreement with CFD was found for both the vorticity and downwash angle downstream the propeller.

Generally speaking, the lesson learned from this activity is the great potential of a mid-fidelity numerical approach for the investigation of interactional aerodynamics problems typical of the novel complex rotorcraft architectures characterizing eVTOL aircraft. As a matter of fact, the most interesting aspect is the quite lower computational effort required by this approach with respect to high-fidelity CFD methods together with the quite good accuracy obtained for the calculation of the aerodynamic performance and flow physics related to the aerodynamic interaction between the propeller and lifting surfaces. Indeed, the whole numerical activity presented in this paper was obtained using a commercial laptop, while classical high-fidelity CFD would require the use of clusters. Consequently, this work would like to indicate the opening of a new scenario for the preliminary design stage of novel rotorcraft configurations such as tiltrotor or eVTOL aircraft. Indeed, mid-fidelity solvers such as DUST showed to be mature to provide fast and accurate solutions for the calculation of the aerodynamic performance of complex rotorcraft vehicles as well as to give a comprehensive understanding and explanation of the physics of interactional mechanisms.

CRediT authorship contribution statement

Claudio Niro: Investigation, Visualization, Writing – original draft. **Alberto Savino:** Conceptualization, Data curation, Formal analysis, Investigation, Methodology, Software, Supervision, Validation. **Alessandro Cocco:** Formal analysis, Methodology, Software, Supervision. **Alex Zanotti:** Formal analysis, Investigation, Methodology, Project administration, Software, Supervision, Validation, Writing – original draft, Writing – review & editing.

Declaration of competing interest

The authors declare that they have no known competing financial interests or personal relationships that could have appeared to influence the work reported in this paper.

Data availability

Data will be made available on request.

Acknowledgements

This research has received no funding.

References

[1] M. Abou-Zeid, A.P. Akkinepally, C.A. Haddad, Contributors, in: C. Antoniou, D. Efthymiou, E. Chaniotakis (Eds.), Demand for Emerging Transportation Systems, Elsevier, 2020, pp. xiii–xiv, https://www.sciencedirect.com/science/article/pii/B9780128150184010020.

[2] S. Roy, A. Maheshwari, W.A. Crossley, D.A. DeLaurentis, Future regional air mobility analysis using conventional, electric, and autonomous vehicles, J. Air Transp. 29 (3) (2021) 113–126, https://doi.org/10.2514/1.D0235.

[3] M. Fu, R. Rothfeld, C. Antoniou, Exploring preferences for transportation modes in an urban air mobility environment: Munich case study, Transp. Res. Rec. 2673 (10) (2019) 427–442, https://doi.org/10.1177/0361198119843858.
[4] J. Yin, S. Ahmed, Helicopter main-rotor/tail-rotor interaction, J. Am. Helicopter Soc. 45 (2000) 293–302, https://doi.org/10.4050/JAHS.45.293.
[5] M. Wentrup, J. Yin, P. Kunze, T. Streit, J.-H. Wendisch, T. Schwarz, J.-P. Pinacho, K. Kicker, R. Fukari, An overview of DLR compound rotorcraft aerodynamics and aeroacoustics activities within the CleanSky2 NACOR project, 2018.
[6] D. Opoku, D. Triantos, F. Nitzsche, S. Voutsinas, Rotorcraft aerodynamic and aeroacoustic modelling using vortex particle methods, in: Proceedings of the 23rd International Congress of Aeronautical Sciences, ICAS, Toronto, Canada, 2002.
[7] G.S. Winckelmans, Topics in vortex methods for the computation of three- and two-dimensional incompressible unsteady flows, Ph.D. thesis, California Institute of Technology, 1989, https://resolver.caltech.edu/CaltechETD:etd-11032003-112216.
[8] Y. Lu, T. Su, R. Chen, P. Li, Y. Wang, A method for optimizing the aerodynamic layout of a helicopter that reduces the effects of aerodynamic interaction, Aerosp. Sci. Technol. 88 (2019) 73–83, https://doi.org/10.1016/j.ast.2019.03.005, https://www.sciencedirect.com/science/article/pii/S1270963818317760.
[9] J. Tan, J. Sun, G. Barakos, Unsteady loads for coaxial rotors in forward flight computed using a vortex particle method, Aeronaut. J. 122 (1251) (2018) 693–714.
[10] J. Tan, T. Zhou, J. Sun, G. Barakos, Numerical investigation of the aerodynamic interaction between a tiltrotor and a tandem rotor during shipboard operations, Aerosp. Sci. Technol. 87 (2019) 62–72.
[11] E.J. Alvarez, J. Mehr, A. Ning, FLOWUnsteady: an interactional aerodynamics solver for multirotor aircraft and wind energy, https://doi.org/10.2514/6.2022-3218, 2022, https://arc.aiaa.org/doi/abs/10.2514/6.2022-3218.
[12] M. Tugnoli, D. Montagnani, M. Syal, G. Droandi, A. Zanotti, Mid-fidelity approach to aerodynamic simulations of unconventional VTOL aircraft configurations, Aerosp. Sci. Technol. 115 (2021) 106804, https://doi.org/10.1016/j.ast.2021.106804, https://www.sciencedirect.com/science/article/pii/S127096382100314X.
[13] T. Sinnige, N. van Arnhem, T.C.A. Stokkermans, G. Eitelberg, L.L.M. Veldhuis, Wingtip-mounted propellers: aerodynamic analysis of interaction effects and comparison with conventional layout, J. Aircr. 56 (1) (2019) 295–312, https://doi.org/10.2514/1.C034978.
[14] T. Sinnige, T. Stokkermans, N. van Arnhem, L. Veldhuis, Aerodynamic performance of a wingtip-mounted tractor propeller configuration in windmilling and energy-harvesting conditions, in: AIAA Aviation 2019 Forum, 2019.
[15] T.C.A. Stokkermans, N. van Arnhem, T. Sinnige, L.L.M. Veldhuis, Validation and comparison of RANS propeller modeling methods for tip-mounted applications, AIAA J. 57 (2) (2019) 566–580, https://doi.org/10.2514/1.J057398.
[16] N. Van Arnhem, Unconventional propeller-airframe integration for transport aircraft configurations, Ph.D. thesis, Delft University of Technology, 2022.
[17] G.H. Cottet, P.D. Koumoutsakos, Vortex Methods: Theory and Practice, Cambridge University Press, 2000.
[18] S. Gallay, E. Laurendeau, Nonlinear generalized lifting-line coupling algorithms for pre/poststall flows, AIAA J. 53 (7) (2015) 1784–1792.
[19] L. Morino, C.-C. Kuo, Subsonic potential aerodynamics for complex configurations: a general theory, AIAA J. 12 (2) (1974) 191–197, https://doi.org/10.2514/3.49191.
[20] M. Tugnoli, D. Montagnani, M. Syal, G. Droandi, A. Zanotti, Mid-fidelity approach to aerodynamic simulations of unconventional VTOL aircraft configurations, Aerosp. Sci. Technol. 115 (2021) 106804, https://doi.org/10.1016/j.ast.2021.106804.
[21] A. Savino, A. Cocco, A. Zanotti, M. Tugnoli, P. Masarati, V. Muscarello, Coupling mid-fidelity aerodynamics and multibody dynamics for the aeroelastic analysis of rotary-wing vehicles, Energies 14 (21) (2021) 6979, https://doi.org/10.3390/en14216979.
[22] T. Sinnige, N. van Arnhem, T.C.A. Stokkermans, G. Eitelberg, L.L.M. Veldhuis, Wingtip-mounted propellers: aerodynamic analysis of interaction effects and comparison with conventional layout, J. Aircr. 56 (1) (2019) 295–312, https://doi.org/10.2514/1.C034978.
[23] G. Gori, T. Davoli, A. Rausa, A. Zanotti, F. Auteri, A. Guardone, Bayesian calibration of a low order aerodynamic model for the design of unconventional tail empennages, in: AIAA AVIATION 2023 Forum, 2023, p. 4422.
[24] M. Drela, Xfoil: an analysis and design system for low Reynolds number airfoils, in: T.J. Mueller (Ed.), Low Reynolds Number Aerodynamics, Springer Berlin Heidelberg, Berlin, Heidelberg, 1989, pp. 1–12.
[25] L.A. Viterna, D.C. Janetzke, Theoretical and experimental power from large horizontal-axis wind turbines, Tech. Rep., Washington Procurement Operations Office, Washington, DC (United States), September 1982.
[26] C. Niro, Numerical investigation of the aerodynamic interactions between a tip-mounted propeller and a wing with deflected flap using the mid-fidelity solver dust, Master's thesis, Politecnico di Milano, 2023.
[27] N. van Arnhem, T. Sinnige, T. Stokkermans, G. Eitelberg, L. Veldhuis, Aerodynamic interaction effects of tip-mounted propellers installed on the horizontal tailplane, in: AIAA Aerospace Sciences Meeting, 2018.